AIAA JOURNAL
Vol. 49, No. 10, October 2011

Effects of Simple Wall-Mounted Cylinder Arrangements on a Turbulent Boundary Layer

Mitchell D. Ryan,* Cecilia Ortiz-Dueñas,† and Ellen K. Longmire‡
University of Minnesota, Minneapolis, Minnesota 55455

DOI: 10.2514/1.J051012

Hot-wire measurements were acquired downstream of a single cylinder and single spanwise arrays of cylinders with height-to-diameter ratio $H/D = 1.5$. The tops of the cylinders were located near the top of the logarithmic region ($z/\delta = 0.13, z^+ = 150$) in a turbulent boundary layer with $Re_\tau = 1200$. Two additional tests used cylinders of half the original diameter with tops located at $z^+ = 150$ and 100. Measurements included velocity profiles and frequency spectra up to 12 diameters downstream. The single cylinder yielded a mean velocity deficit that extended from $z^+ = 20$ to 200 and a redistribution of the root-mean-square velocity away from the wall toward the top of the cylinder with a corresponding increase in the power spectral density over a broad frequency range. Cylinder arrays with 3*D* and 6*D* spanwise spacing yielded significant wake interactions producing mean velocity deficits and rms values greater than those observed at equivalent distances downstream of a single cylinder. The largest mean deficits and root-mean-square velocities occurred in the log region at midspacing between cylinders. No dominant frequency was observed in these regions; however, a significant spectral peak was observed in the wake of a single cylinder. Significant wake interaction effects extended to the top of the log region but not beyond.

Introduction

IN MANY aerospace applications it is desirable to manipulate or control turbulent boundary layers in order, for example, to improve aerodynamic or combustion performance, locally increase or decrease skin friction or heat transfer, or reduce drag and noise. Turbulent boundary layers are known to contain coherent vortical structures or eddies, which have been characterized as hairpins, arches, horseshoes, and cane-shape vortices. These eddies are believed to be one of the main self-sustaining mechanisms in wall-bounded turbulence [1]. Thus, a possible method to modify the behavior of turbulent boundary layers is to manipulate or alter the organization of these coherent structures.

In particle image velocimetry (PIV) studies, Adrian et al. [2] and Tomkins and Adrian [3] demonstrated the preponderance of hairpin signatures in both the logarithmic and outer regions of turbulent boundary layers. The hairpin signature pattern consists of vortex cores with high values of swirling strength organized coherently in the streamwise direction in groups or packets above regions with high Reynolds shear stress ($u'w' < 0$) and low speed ($u' < 0$) [2,4]. These patterns have been shown to be both statistically relevant and important; i.e., hairpin packets make a significant contribution to the Reynolds stress in the logarithmic region, and therefore to the turbulence transport and production near the wall, while occupying a relatively small cross-sectional area within the boundary layer [4]. These recent studies may be used as guidelines for the scales and possible mechanisms that might potentially result in more efficient manipulation of turbulent boundary layers. For instance, based on these studies, the logarithmic region, where hairpins and hairpin packets signatures are prevalent, appears to be a location of particular interest to attempt an effective manipulation of the hairpin packet structure.

In the current investigation, wall-mounted cylinders smaller than the boundary-layer thickness but large enough to protrude into the logarithmic region are used to modify a turbulent boundary layer in an attempt to affect the organization of the coherent vortical structures. The cylinders investigated herein have an aspect ratio, AR = 1.5 (AR = H/D, where H is the cylinder height and D is the cylinder diameter), low blockage ratio of no more than 1% (ratio of the frontal area of the cylinders to the tunnel cross-sectional area), and are fully immersed in a turbulent boundary layer with $Re_\tau = 1200$ such that the ratio of cylinder height to boundary-layer thickness, H/δ, is approximately 0.13, corresponding to $H^+ = Hu_\tau/\nu = 150$ (where u_τ is the wall friction velocity and ν is the kinematic viscosity). Therefore, the cylinders extend well into the logarithmic region or into the zone containing the bulk of the coherent eddies. The effects of individual cylinders and single spanwise arrays with three to six diameter spanwise spacing are evaluated by examining velocity statistics downstream.

It is clear from previous studies that the flow structure downstream of wall-mounted cylinders (finite length cylinders with one free end) in crossflow is complex, due to the number of parameters that can affect the flow. In general, the flow downstream of wall-mounted cylinders can be characterized by tip vortices formed by the shear layer generated at the free end, Kármán vortices along the majority of the height (akin to those in the flow past cylinders of infinite length [5,6]), and a horseshoe vortex system near the base of the cylinder [7]. Clearly, the geometrical parameters of the cylinder and the characteristics of the incoming flow will have a profound effect on these downstream structures. Based on previous literature, three parameters that appear to affect the flow significantly are the aspect ratio, AR, the nature of the incoming flow: laminar or turbulent, and the height of the cylinder with respect to the boundary layer, characterized here by H/δ (where δ is the boundary-layer thickness).

Since our goal is to perturb the organization of vortical structures within a turbulent boundary layer, we are interested in wall-mounted obstacles that reach into the logarithmic region but not beyond, i.e., with low H/δ values, and that do not obstruct the flow significantly, i.e., a sparse array arranged in a single spanwise row. Previous studies of the flow over canopies [8–10] and flow over general surface roughness, [11] wall-mounted obstacles, or roughness elements have H/δ values similar to those studied in this paper. However, the considerable streamwise extent of the canopy or roughness arrays yields perturbations and flowfields that are significantly different

Received 14 October 2010; revision received 25 April 2011; accepted for publication 27 April 2011.

*Research Assistant, Department of Aerospace Engineering and Mechanics.
†Postdoctoral Associate, Institute for Mathematics and its Applications. Member AIAA.
‡Professor, Department of Aerospace Engineering and Mechanics, 110 Union Street SE. Member AIAA.

from those caused by a single row of obstacles as described in this paper, and therefore these studies are not reviewed here. In addition, we are interested in a boundary layer that is already turbulent as opposed to laminar or transitional. If the incoming boundary layer is laminar (e.g., Duriez et al. [12] investigated a single spanwise array of cylinders with similar parameters, AR = 0.75, $H/\delta = 0.5$–0.75, and a spanwise spacing of three diameters), the resulting flow is also significantly different from the present case in that the cylinders may promote instabilities and eventual transition to turbulence.

Obstacles with low H/δ have been used previously in studies of turbulent boundary-layer manipulation for the purpose of reducing viscous drag [13,14]. Most relevant to this paper are a few studies that have directly investigated the effect of specific types of obstacles on the coherent structures in the turbulent boundary layer [15–19]. Corke et al. [15,16] used wall parallel-plates with a chord of 0.9δ located in the range $0.1 < H/\delta < 0.8$ to manipulate a turbulent boundary layer with $Re_\theta \sim 3500$. Hot-wire measurements and flow visualization carried out up to 17δ downstream of the plates revealed a reduction in the streamwise turbulence intensity near the wall, i.e., $z^+ < 100$. Wark et al. [17], using similar obstacles, found that the plates had a small effect on the frequency of occurrence of Reynolds stress producing events (such as ejections $u'w'$) but that interestingly, the return of the boundary layer to its undisturbed condition occurred more than 100 boundary-layer thicknesses downstream of the plates. Guezennec and Nagib [18] provided details on the various mechanisms occurring downstream of these types of obstacles and found that the plates attenuate turbulent velocity fluctuations by inhibiting interaction between the flow above and below the wake of the plates. They observed that the effect on the streamwise turbulence intensity and Reynolds stress profiles ($u'w'$) relaxes after 20–40 boundary-layer thicknesses but that the attenuation of the normal velocity component and its fluctuations persist up to 100–150δ. Schofield and Logan [19] investigated the flow surrounding obstacles in cross flow (mostly prisms and fences) completely immersed in a turbulent boundary layer ($0.3 < H/\delta < 1$). They found that, shortly after the reattachment location, the maximum velocity deficit moves away from the wall and that the decay of this maximum velocity deficit scales with the boundary-layer thickness, δ, and not with the obstacle dimensions. Although the obstacles used in these studies were mostly two dimensional (i.e., "infinite" span) the findings suggest that obstacles fully immersed in a turbulent boundary layer and with low H/δ values can have a large effect on the structure of the turbulent boundary layer and that this effect may persist for a long distance downstream.

The investigations of wall-mounted cylinders immersed within a turbulent boundary layer are relatively few, and the majority of these studies focus on the detailed flow surrounding a single cylinder or the near-wake region of a single cylinder ($x/D \leq 5$, where x is the streamwise coordinate) [20–26]. From these studies, it is clear that the aspect ratio, AR, and the height of the cylinder with respect to the boundary-layer thickness, H/δ, although not necessarily independent, both affect the resulting flowfield characteristics.

First, the aspect ratio of the cylinders, AR, will have a significant effect on the wake structure. Sumner et al. [20] carried out an experimental investigation on the wake structure behind wall-mounted cylinders partly immersed in a turbulent boundary layer. Those authors found that the flow past a cylinder with AR = 3, corresponding to $H/\delta \sim 1.2$, resulted in a different wake structure than the flow past cylinders with higher aspect ratios (AR = 5, 7, 9) and thus higher H/δ (up to 3.45) for a constant cylinder diameter ($Re_D \sim 6 \times 10^4$ based on freestream velocity). For cylinders with low aspect ratio, AR $\leq$ 2–3, the free-end shear layer and resulting tip vortices dominate the near wake, and it was found that the resulting downwash suppresses both the Kármán-type and horseshoe vortices. Therefore, Kármán vortex shedding and its associated frequency measured for the higher-aspect-ratio cylinders, were not observed for the cylinder with AR = 3 [20]. For cylinders with higher aspect ratio, AR > 3–4, corresponding to $H/\delta \gg 1$ and $Re_D \sim 1.1 \times 10^4$ based on freestream velocity, Wang et al. [21] found that the effects of the free-end shear layer are confined to the tip region so that the near-wake is dominated by Kármán-type vortices and horseshoe vortices.

Second, the height of the cylinder with respect to the turbulent boundary layer, H/δ, will affect the development of the wake structures. Wang et al. [21] investigated the near-wake effect ($x/D < 5$) of three different boundary-layer conditions, laminar ($H/\delta = 10$) and turbulent ($H/\delta = 5$ and 2.63) on the flow past a wall-mounted square rod with a high aspect ratio AR = 5. These authors found that the flow downstream included both tip vortices and Kármán-type vortices. The strength of the horseshoe vortex system (in particular, the upwash flow directly behind the rod) was shown to increase with decreasing H/δ. Similar results were obtained by Sakamoto and Arie [22] and Park and Lee [23] for $Re_D \sim 2$–4×10^4 based on freestream velocity. Hain et al. [24] characterized the flow over the tip of a wall-mounted cylinder with AR = 2 and $Re_D \sim 12 \times 10^4$ based on freestream velocity using tomographic PIV. These authors found that the flow over the tip of the cylinder is quite unsteady, with vortex shedding Strouhal numbers varying from as small as $St = fD/U = 0.014$ to $St = 0.2$. However, the ratio of the cylinder height to boundary-layer thickness (H/δ) was 8.7, and thus specific effects of the wall boundary layer on the flow near the cylinder tip were not investigated. In contrast, Castro and Robins [25] investigated the near wake ($x/D < 5$) behind a cube with $H/\delta = 0.1$ and $Re_H \sim 4 \times 10^3$ based on freestream velocity embedded in a turbulent boundary layer. They found that the wake decayed completely by $6H$ but that the decay rate was a strong function of the upstream turbulence and shear. For example, as H/δ was increased above 0.1, such that the upstream turbulence intensity at height H was decreased, the length of the recirculation zone behind the cubes increases; this effect is due to the larger separated shear layers on the top and sides of the cube as inferred by the authors from pressure measurements. Tomkins [8] investigated the flow downstream ($x/D \leq 10$) of single cylinders and hemispheres with AR < 2 that were entirely immersed in a turbulent boundary layer with $H/\delta \approx 0.05$–0.15 and $Re_D \sim 5 \times 10^3$ based on freestream velocity. According to the Reynolds number of that investigation, $Re_\tau = 2216$, the cylinders and hemispheres were also immersed in the logarithmic region of the boundary layer with $H^+ \approx 100$–300. Tomkins [8] concluded that the even though the peak of swirling strength measured downstream occurs at approximately midheight for all elements, a significant swirling strength is observed downstream of the hemisphere for heights up to $2H$ or $H^+ \approx 400$, which corresponds to approximately the top of the log region. Furthermore, the author found that the wake downstream of the hemisphere was characterized by a greater number of strong vortices (quantified using swirling strength) relative to the cylinder wake and that the upstream turbulence disrupts shedding frequency such that no dominant frequency was measured. It is clear that the flow past a cylinder entirely immersed in a turbulent boundary layer differs significantly from the flow past a cylinder that extends beyond δ.

In the case of a single spanwise array of wall-mounted cylinders, the two main parameters, aspect ratio and the height of the cylinder with respect to the boundary-layer thickness, H/δ, must also play important roles. However, it is expected that the element arrangement may lead to additional interactions in the wake. Park and Lee [26] investigated the effect of spanwise spacing on the flow downstream of two side-by-side cylinders with AR = 6 immersed in a turbulent boundary layer ($H/\delta \sim 0.85$, $Re_D = 20,000$). They found that, for the largest spacing investigated, $2D$, measurements at the half cylinder height ($z/H = 0.5$, $z/\delta = 0.42$) revealed no interaction between adjacent cylinders. Tomkins [8], in turn, found that two wall-mounted hemispheres with a spanwise spacing of $1.3D$, yielded wake interactions such that the maximum velocity deficit was much larger than that downstream of single element counterparts. The maximum velocity deficit was located in the midplane between the two hemispheres extending up to approximately $z/H = 1.5$ and was sustained for more than five diameters downstream. Tomkins [8] measurements did include regions closer to the wall: $z^+ > 20$ to $z/\delta < 0.72$. Tomkins [8] also concluded that, as with the single element, the boundary-layer turbulence impedes any well-defined periodic vortex shedding off of the elements and that those elements smaller than the upstream turbulence integral length scale will disrupt the flow leading to a smaller length scale downstream. From previous

studies, that of Tomkins [8] appears most relevant. However, that author studied only one case of two wall-mounted elements with a small spanwise spacing.

As described above, the aim of the current investigation is to manipulate or alter the organization of coherent structures in a turbulent boundary layer by inserting a single spanwise array of obstacles into the log region. The primary objective addressed in this paper is to determine the effect of spanwise obstacle spacing on the resulting velocity field. A secondary objective is to comment on the effect of obstacle geometric parameters (H/δ and AR) on the resulting fields. For these purposes, wall-mounted cylinders fully immersed in a turbulent boundary layer but extending well into the log region, $H/\delta = 0.13$ ($H^+ = 150$) and with an aspect ratio AR $= 1.5$, are investigated as single elements and in spanwise arrays with $3D$–$6D$ spacing. Cylinders were chosen because of their relatively simple geometry. Additional tests were carried out using wall-mounted cylinders with half the original diameter and with heights of $H^+ = 150$ corresponding to an aspect ratio of (AR $= 3.0$) and with a height of $H^+ = 100$ (corresponding to an aspect ratio of AR $= 2.0$).

Apparatus and Methods

Hot-wire measurements were taken in a turbulent boundary layer using a suction type, zero-pressure gradient wind tunnel of rectangular cross section (0.3 m height by 1.2 m span). The ceiling height in the tunnel is adjustable at four locations to allow for boundary-layer growth while maintaining a nominally zero-pressure gradient. The gradient was set by trial and error by traversing a pitot tube in the freestream along the length of the test section and adjusting the ceiling to obtain a uniform freestream velocity to within $\pm 0.5\%$. A trip wire 3.3 m upstream of the measurement location initiated the turbulent boundary layer, which developed on the smooth aluminum plates that make up the tunnel floor. At the measurement location, the boundary-layer thickness was approximately $\delta = 72$ mm and the mean freestream velocity was $U_\infty = 6$ m/s or, equivalently, $U_\infty^+ = U_\infty/u_\tau$ was 24. All quantities denoted with the superscript $+$ are normalized using the wall friction velocity u_τ determined by the Clauser chart method, and the kinematic viscosity υ. The resulting Reynolds number based on the boundary-layer thickness and freestream velocity was $Re_\delta = 28,800$; also, $Re_\theta = 2800$ and $Re_\tau = 1200$. Hot-wire measurements indicated that the freestream rms velocity was less than 0.2% of the freestream velocity.

Spanwise arrays of prefabricated stainless steel smooth cylinders (dowel pins) with height $H/\delta = 0.13$ ($H^+ = 150$) and aspect ratio AR $= 1.5$ ($D^+ = 100$, $Re_D = 1700$), using the mean velocity at the top of the cylinder location in the undisturbed profile) were mounted vertically in a single spanwise row of 11 or more cylinders and were used for all tests with one exception: the tests depicted in Fig. 1c use thinner cylinders with $H^+ = 150$ and $D_2^+ = 50$ ($Re_D = 850$) and also thinner, shorter cylinders with $H_2^+ = 100$ and $D_2^+ = 50$ ($Re_D = 800$). The cylinders were glued to the wall using a drop of cyanoacrylate on the end of each cylinder. A laser-cut plastic jig held the cylinders in place for gluing and ensured a straight line across the span with precise spacing. The maximum blockage created by the cylinders (ratio of the frontal area of the cylinders to the tunnel cross-sectional area) was 1% and if only the boundary-layer cross-sectional area (δtimes tunnel span) is included, the blockage was approximately 4.4%. Hot-wire measurements were collected downstream of rows of cylinders with $3D$ and $6D$ center-to-center spanwise spacing, as well as downstream of a single cylinder. A summary of the test locations is shown in Fig. 1. In subsequent discussions, the x, y and z axis are aligned with the streamwise, spanwise, and wall-normal directions, respectively, and the origin is defined at the wall position of the axis of the central cylinder. The first downstream measurement location was selected to be at $x/D = 4$ to ensure that the flow had reattached; this value was selected based on previous studies by Castro and Robins [25], Park and Lee [26], and Sumner et al. [20]. The reattachment was further verified using the velocity profiles at this downstream location that extended relatively close to

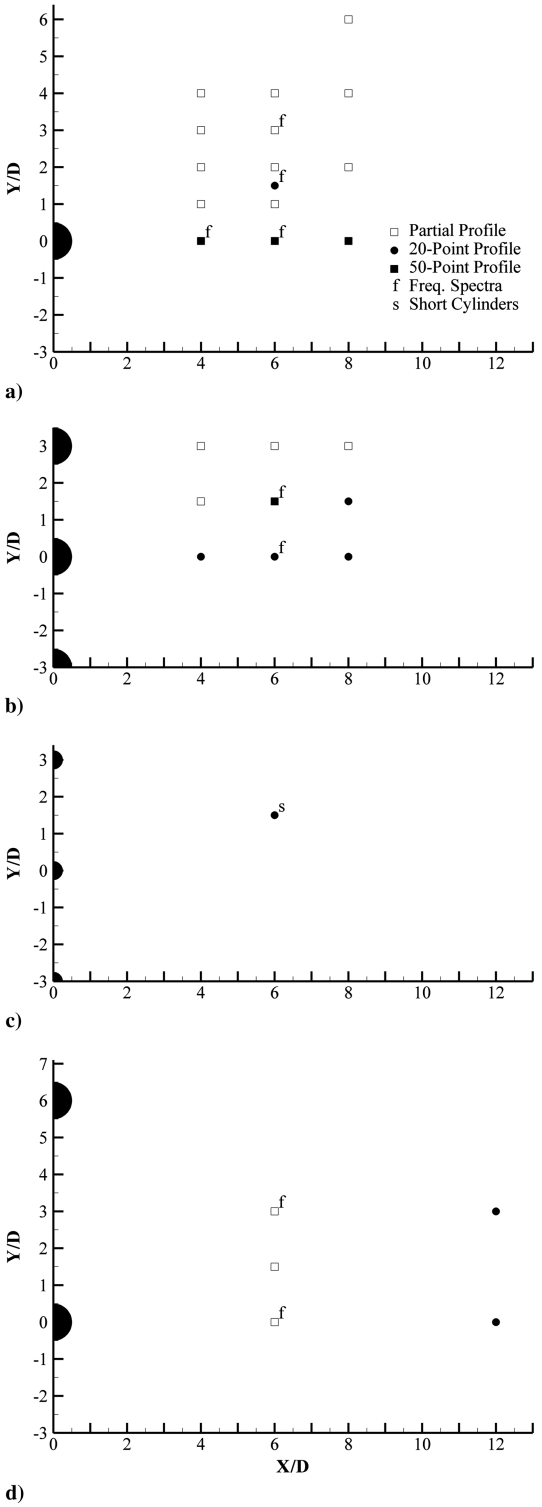

Fig. 1 Hot-wire measurement locations downstream of a) a single cylinder, b) an array of cylinders with $3D$ spanwise spacing, c) an array with the same physical spacing as the $3D$ array but with cylinders of half the original diameter, and d) an array of cylinders with $6D$ spanwise spacing. Full velocity profiles consist of either 20 or 50 logarithmically spaced points (up to $z^+ = 1600$), partial profiles consist of only five points (between $z^+ = 20$ and $z^+ = 100$). All frequency spectra were acquired at $z^+ = 100$ and normalized by inner scales. These data were also used to determine the turbulence integral length scale. In part c, two profiles were acquired, one with cylinders of $H^+ = 150$ as usual and the other marked as "Short Cylinders" with $H_2^+ = 100$. In both cases, the cylinders have $D_2^+ = 50$, rather than the usual $D^+ = 100$. The symbol size represents the uncertainty in positioning the probe in the spanwise and streamwise directions.

the wall. The hot-wire probe's sensing element was a 6 μm tungsten wire, 1.2 mm long ($l^+ = 20$), oriented parallel to the wall and perpendicular to the flow direction. Constant-temperature anemometry was used with an overheat ratio of 1.7 for all tests, and the freestream temperature was nominally constant throughout each test. The hot-wire was calibrated in the freestream with a pitot tube over a velocity range of 0 to 16 m/s. A fifth-order polynomial curve fit was used to obtain $U = f(V)$ for each test. The wire was calibrated before and after each data-collection session to ensure data precision. When the freestream velocity was measured at the end of each session using each of these calibrations, the difference, or drift, was never more than 2% of the freestream velocity.

The probe was mounted on a wall-normal traverse to enable collection of boundary-layer profiles at various locations downstream of the cylinder arrangements (Fig. 1). A pair of synchronized stepper motors connected to a computer control system operated the traverse in the wall-normal (z) direction. Profiles consisted of either 20 or 50 logarithmically spaced points from $z^+ = 8$ to $z^+ = 1600$. Data were obtained by sampling at 1 kHz for 2 min at each point, which resulted in a minimum of 4000 statistically independent samples per data point. The profiles were taken from the wall upward; streamwise and spanwise adjustments were performed manually. The uncertainty in the wall-normal positioning was estimated at ± 4 wall units or ± 0.25 mm. The uncertainty in the streamwise and spanwise positioning was less than ± 10 wall units or ± 0.6 mm and is represented by the symbol size in Fig. 1 (see caption). The uncertainty in the reported values in the mean streamwise velocity profiles was estimated using the root sum of squares method to combine the uncertainty due to the calibration and that due to the variance in the independent samples [27]. This uncertainty was less than $\pm 2.2\%$ of the freestream velocity for all tests and is equivalent to twice the symbol size in the mean velocity plots. The uncertainty in the rms measurements was evaluated in a similar way and found to be less than $\pm 0.12\%$ of the freestream velocity for all tests, which is equivalent to the symbol size in the rms velocity plots.

The integral length scale was computed as

$$L = \bar{U} \int_0^{t_0} R(t)\, \mathrm{d}t \tag{1}$$

where $R(t)$ denotes the normalized autocorrelation function of the measured velocity with a time shift t (i.e., the correlation of the velocity with a time-shifted, or sample-shifted, version of itself, normalized so that the correlation returns unity when $t = 0$). In Eq. (1), t_0 represents the first zero crossing of $R(t)$, i.e., the smallest t such that the velocity does not correlate positively with itself, and $\bar{U}$ denotes the mean velocity at the measurement location. This process gives the approximate scale of the largest coherent structures passing the measurement location. Frequency spectra were computed using Welch's method for power spectral density (PSD) calculations and normalized by inner scales. A window size of 4096 Hz was used; however, using a different window size did not significantly affect the results. Separate data were collected for the spectra measurements and were also used, when available, for length-scale calculations. The sampling rate was 40 kHz (chosen by trial and error to capture the highest-frequency content) and 240,000 samples were collected. The cutoff frequency of the system was determined using a square-wave test and found to be a least 120 kHz for all tests. The wall-normal location for these measurements was chosen at $z^+ = 100$ because many of the full profiles had maximum rms velocity at this location.

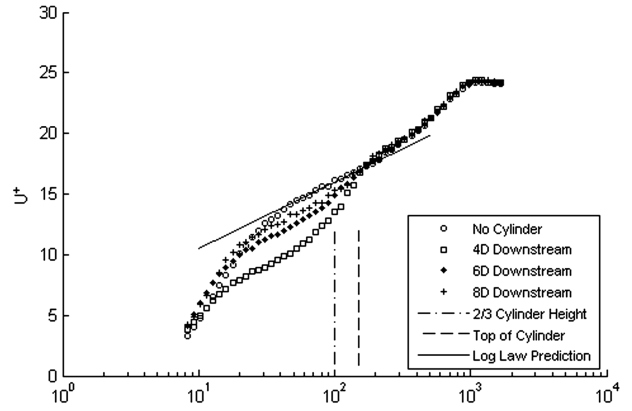

a) Mean velocity

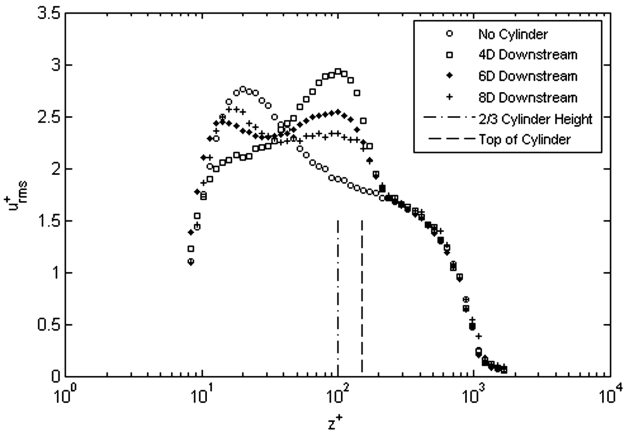

b) RMS velocity

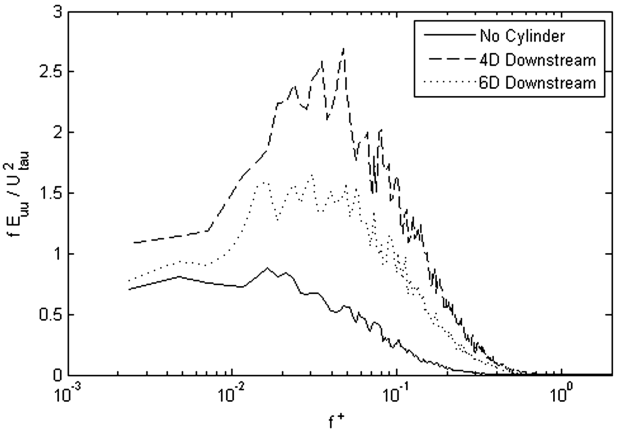

c) Frequency spectra

Fig. 2 Velocity profiles and frequency spectra behind a single cylinder at various downstream locations with no spanwise offset ($y/D = 0$): a) mean velocity with log law prediction of the undisturbed case using $k = .42$, $B = 5.0$, b) rms velocity, and c) frequency spectra at $z^+ = 100$ normalized by inner scales. In all figures, the symbol size in the mean velocity plots represents half of the measurement uncertainty, while in the rms velocity plots it represents the total uncertainty.

Results and Discussion

Single Cylinder

The development of the flow directly downstream of a single cylinder is shown in Fig. 2 at streamwise locations $x/D = 4, 6$, and 8. Mean and rms velocity profiles are shown in Figs. 2a and 2b, respectively, and the normalized frequency spectra at the wall-normal location $z^+ = 100$, corresponding to the 2/3 cylinder height (indicated by the dot-dashed line in all figures), are shown in Fig. 2c. The dashed line in the figures at $z^+ = 150$corresponds to the height of the cylinder. In Fig. 2, and all subsequent figures, profiles of the undisturbed case (no cylinder) are included for reference. The size of the symbols used in the mean velocity plots represents roughly half of the measurement uncertainty, while in the rms plots, the symbol size represents the total uncertainty. In Fig. 2a, a log law line corresponding to

$$U^+ = \frac{1}{k}\ell_n(z^+) + B \tag{2}$$

with values for $k = 0.42$ and $B = 5.0$ is included. The log law line agrees well with the undisturbed mean velocity profile in the range $z^+ = 40$ to $z^+ = 200 = 0.2\delta^+$, as predicted by Pope [28].

Downstream of a single cylinder, at $x/D = 4$, the reduction in mean velocity (velocity deficit) extends from the near-wall region, i.e., $z^+ = 20$, up to the top of the log region at $z^+ = 200$. The velocity deficit decays slowly with increasing downstream distance and by $x/D = 8$, the mean velocity profile appears to have returned to the undisturbed condition except for a small region near the 2/3 cylinder height, $z^+ = 100$, where a small deficit is still observed and below $z^+ = 20$, where a small surplus is observed. This surplus in the near-wall region is observed in several cases and is discussed in greater detail below.

Figure 2b shows that the rms velocity reaches a maximum of $u_{\text{rms}+} = 2.8$ at $z^+ = 20$ for the undisturbed case, which agrees well with the values published by Pope [28] and Wei and Willmarth [29] for a channel flow at $Re_\delta = 22,776$. In the perturbed profile at $x/D = 4$, the rms velocity exhibits a peak of slightly larger magnitude at $z^+ = 100$, which coincides with the 2/3 cylinder height. The increase in rms away from the wall extends to approximately the top of the log layer, i.e., $z^+ = 200$. With increasing downstream distance, $x/D = 6$, the rms peak at $z^+ = 100$ decreases as the peak at $z^+ = 20$ begins to relax toward the undisturbed condition. At $x/D = 8$, the maximum value has reverted to the near-wall region, although the profile still shows a clear perturbation. These results indicate that the cylinder acts to decrease the near-wall streamwise turbulence while simultaneously and significantly increasing the streamwise turbulence near the top of the cylinder and up to the top of the log layer. This effect decreases with downstream distance as the boundary layer begins to recover its undisturbed form. The normalized frequency spectra at the 2/3 cylinder height $z^+ = 100$, shown in Fig. 2c, show an increase in normalized power spectral density across most of the frequency range when the undisturbed and disturbed conditions are compared. At $x/D = 4$, the increase is as much as fivefold, which is consistent with the high rms peak observed in Fig. 2b. By $x/D = 6$, the normalized power spectral density remains higher than the undisturbed case but noticeably less than at $x/D = 4$, which agrees with the reduction of the rms velocity with streamwise distance at this wall-normal location.

Figures 3–5 show the development of the flow at various spanwise offsets, up to six diameters from the cylinder axis, at streamwise locations $x/D = 4$, 6, and 8. Mean velocity profiles, shown in Fig. 3, indicate that at $x = 4D$ (Fig. 3a), the velocity deficit in the log region is greatest directly downstream of the cylinder. The velocity deficit decreases in the spanwise direction, as expected, indicating that the wake extends to less than $3D$ from the cylinder axis. (The data for a $3D$ offset overlap the unperturbed data.) At $x/D = 6$ (Fig. 3b), the velocity deficit directly behind the cylinder reduces, and the wake still extends to approximately $3D$ in the spanwise direction. However, at this streamwise location, the wake exhibits a velocity deficit at a spanwise offset of $y/D = 1$ that is similar to that seen at $x/D = 4$, $y/D = 1$. By $x/D = 8$ (Fig. 3c), the mean velocity profiles have approached the undisturbed condition for all spanwise locations, suggesting the wake has decayed substantially. Note that the velocities measured at offsets of $4D$ and $6D$ match the undisturbed case within uncertainty. These results are consistent with those observed by Castro and Robins [25] for a single cube immersed in a turbulent boundary layer with $H/\delta = 0.1$. They found that the wake decayed completely by $x/H = 6$ but that the decay rate was a strong function of the upstream turbulence and shear.

The rms velocity profiles (Fig. 4) at spanwise offsets from the cylinder axis show similar trends to those observed for the mean velocity profiles with a few additional observations. In Fig. 4, it is interesting to note that as the probe is moved in the spanwise direction, rather than a steady progression of decreasing rms velocity in the vicinity of $z^+ = 100$ and a slow increase of rms near $z^+ = 20$ as seen directly downstream of the cylinder for increasing downstream distance (Fig. 2b), the rms profile exhibits an intermediate case of a single broad peak extending at least up to the 2/3 cylinder height, $z^+ = 100$, for all streamwise locations. At $x/D = 4$ (Fig. 4a) the broad peak is observed at a spanwise offset of $y/D = 1$. By

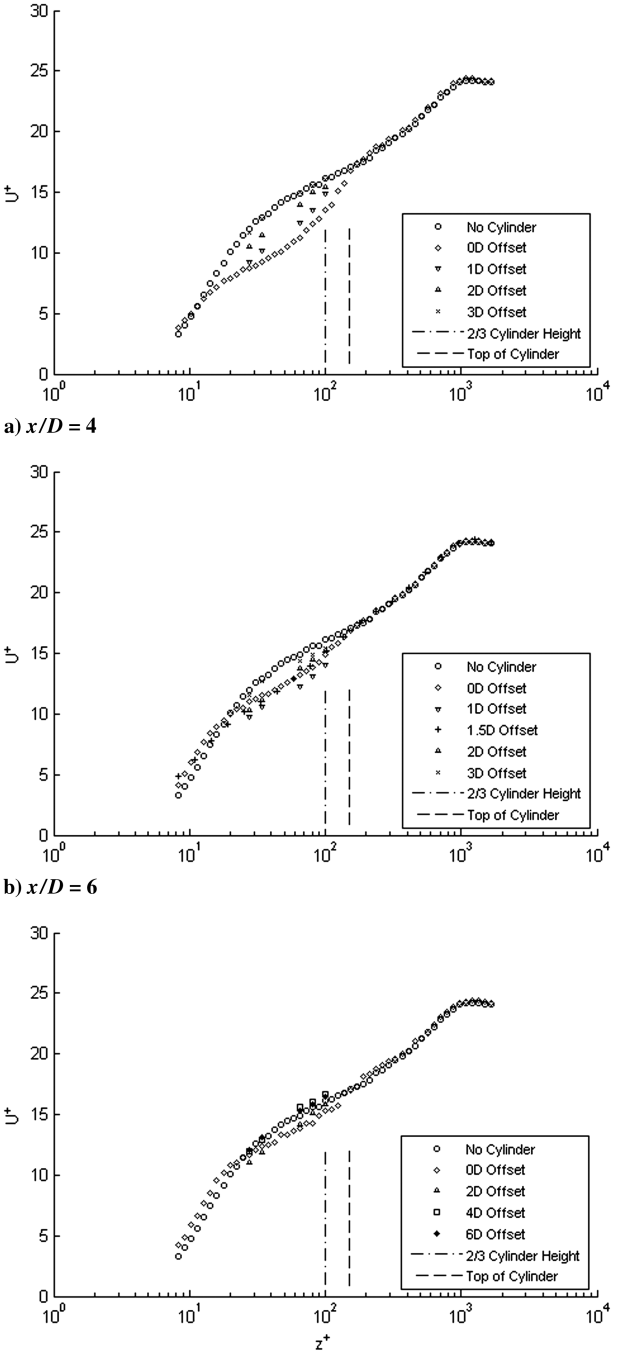

a) $x/D = 4$

b) $x/D = 6$

c) $x/D = 8$

Fig. 3 Mean velocity profiles behind a single cylinder at various downstream locations and spanwise offsets.

$y/D = 2$, the rms profile is shifting toward that of undisturbed case, and overlaps the undisturbed case by $y/D = 3$ as was also true for the mean velocity in Fig. 3a. At $x/D = 6$ (Fig. 4b) no change is observed at $y/D = 1$ relative to the profile at $y/D = 0$. The broad peak is observed at $y/D = 1.5$ and to a lesser extent at $y/D = 2$, followed by a return to the undisturbed condition by $y/D = 3$. By $x/D = 8$, the broad peak occurs near $y/D = 2$ and the profile nearly returns to the undisturbed condition by $y/D = 4$. The single broad peak of rms velocity at $x/D = 8$, $y/D = 2$, possibly indicates a long-lasting effect on the streamwise (and possibly spanwise) turbulent fluctuations at a spanwise offset.

The normalized frequency spectra at the 2/3 cylinder height, $z^+ = 100$ and $x/D = 6$ (Fig. 5) show a return to the undisturbed condition by $y/D = 3$, which agrees with the observations in the mean (Fig. 3b) and rms (Fig. 4b) velocity profiles. At $y/D = 1.5$,

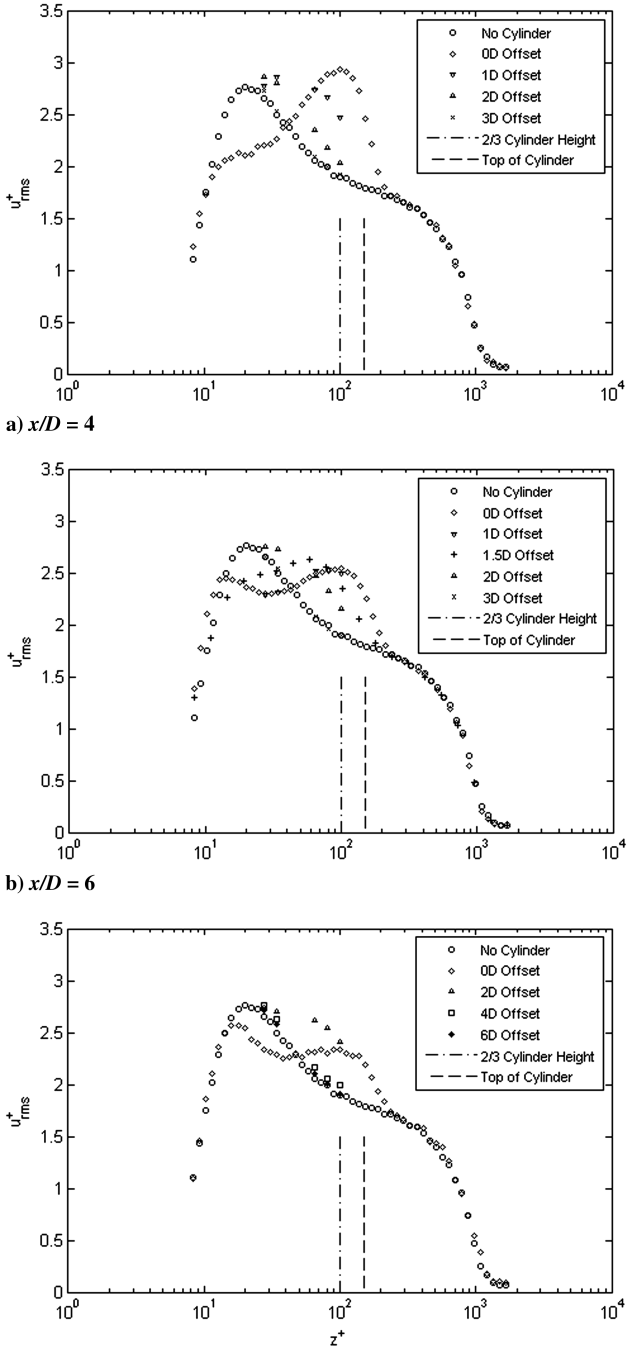

Fig. 4 RMS velocity profiles behind a single cylinder at various downstream locations and spanwise offsets.

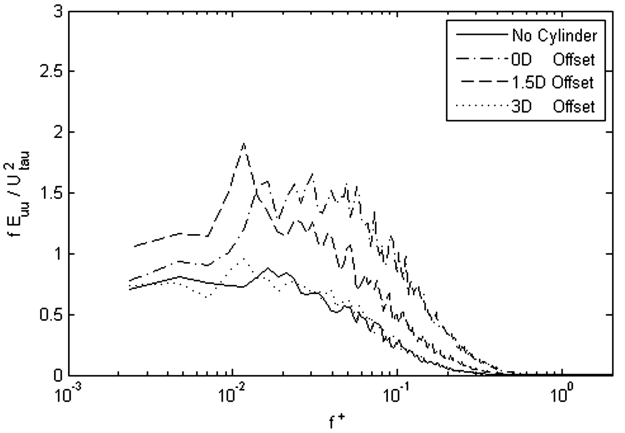

Fig. 5 Normalized frequency spectra behind a single cylinder at $z^+ = 100$, $x/D = 6$ and various spanwise offsets.

there is less power density across most of the frequency range when compared with the spectrum at $y/D = 0$, which agrees with the lower rms value at $z^+ = 100$ in Fig. 4b. Additionally, at $y/D = 1.5$, there is a significant peak at $f^+ = 0.012$ corresponding to a Strouhal number $St = fD/U = 0.08$, where U is the normalized mean velocity at $z^+ = 100$ in the undisturbed profile. The peak suggests possible vortex shedding off the cylinder. At $y/D = 0$, there is a peak at $f^+ = 0.023$, approximately double the frequency of, and potentially related to, the significant peak at $y/D = 1.5$, but this peak does not dominate.

The behavior of a long-lasting increase in rms velocity near the top of an obstacle but not beyond the top of the log region (corresponding here to $z^+ < 200$) was also observed by Tomkins [8] who reported an increase in swirling strength beyond the element height (i.e., $H^+ \approx 100$–300) and up to $H^+ = 400$ corresponding also to the top of the log region for the Reynolds number investigated, $Re_\tau = 2216$. Tomkins [8] also reported vortex shedding, although not highly periodic, downstream of both hemispheres and cylinders and conjectured that the upstream turbulent boundary layer impedes any well-defined periodic vortex shedding off of elements. This is consistent with the absence of any noticeable peaks in most of the current normalized frequency spectra (Figs. 2c and 5) taken at $z^+ = 100$. Sumner et al. [20] observed that the distinct Kármán shedding frequency measured for high-aspect-ratio cylinders, AR > 5, was not observed for a cylinder with AR = 3. However, closer inspection of their data in the near-wake region ($x/D = 3$, $y/D = 0$) below the half cylinder height revealed a weak peak with a Strouhal number of 0.14. Sumner et al. [20] attributed this frequency to the tip vortex, which generates a downwash extending to the wall (before $x/D = 3$) and which in turn suppresses the Kármán vortex shedding for that AR. In the current investigation, the hot-wire probe was moved manually through a range of locations, while the hot-wire signal was monitored to search for further evidence of periodic shedding but no obviously dominant frequency was observed in the output. It should be noted also that the peak observed in Fig. 5 was not dominant enough to be obvious while observing the hot-wire signal manually.

The integral length-scale calculations (Eq. 3) revealed that the largest turbulent structures passing the $z^+ = 100$ location for the undisturbed case are approximately $L^+ = 400$, or four cylinder diameters. This scale also persists in the wake of the single cylinder wherever the rms and mean velocity profiles do not differ significantly from the undisturbed condition. However, when the mean or rms velocity was clearly altered, the integral length scale at $z^+ = 100$ downstream of the single cylinder was reduced to $L^+ = 250$–300, or 2.5–3 cylinder diameters, suggesting some significant effect on the turbulent structure. This result agrees with Tomkins [8] who reported that wall-mounted elements with dimensions smaller than the scale of the upstream turbulence would act to decrease the turbulence length scale. It should be noted that this reduction in length scale could be due largely to an increase of smaller-scale turbulence caused by the cylinders and does not necessarily suggest that the larger scales have been reduced in size.

To summarize, these results show that a single cylinder perturbs a turbulent boundary mainly over the range $z^+ = 20$ to $z^+ = 200$ (which is equivalent to the top of the log region or about 4/3 the cylinder height). A key effect is an increase in the rms values with a peak at $z^+ = 100$, the 2/3 cylinder height, resulting in an increase of normalized power spectral density and a reduction of integral length scale. This effect was observed up to $x/D = 8$ and $3D$ in the spanwise direction. These results are evidence of a long-lasting effect (at least $x/D = 8$) on the streamwise rms velocity and integral length scale and hence a possible modification of the structure of the turbulent boundary layer. To further explore these effects and possible modifications to eddy organization, spanwise arrays of wall-mounted cylinders were investigated.

Cylinder Arrays

Cylinder arrays with two spanwise spacings, $3D$ and $6D$, were investigated. Figure 6 shows the effect of cylinder-array spacing on the mean and rms velocity profiles at $x/D = 6$. Single-cylinder data are included for comparison. In Fig. 6a (profiles taken directly downstream of a cylinder, $y/D = 0$), the mean and rms velocity profiles resemble those downstream of the single cylinder for both $3D$ and $6D$ spacing. However, at the midspacing offset (Fig. 6b), the profiles for the $3D$ and $6D$ spacing differ significantly. For the array with $6D$ spacing, the cylinders appear to behave like independent elements such that the profiles resemble those behind the single cylinder. The normalized frequency spectra collected for the $6D$ array indicated in Fig. 1 (not plotted) also very closely resemble those collected at similar locations downstream of a single cylinder. With a spanwise spacing of $3D$ however, a larger mean velocity deficit and a higher rms velocity peak at $z^+ = 100$ are observed in the profiles at $y/D = 1.5$, the midspacing location. This suggests significant spanwise interactions between cylinder wakes, and thus the $3D$ spacing cylinder array was investigated further.

It is interesting to note that neither cylinder array has an observable effect on the mean or rms velocity at wall-normal locations exceeding the height of the log region ($z^+ = 200$) or $4/3$ the cylinder height. This result differs from the behavior observed in canopy flows in which the rms velocity peak occurs at the vegetation height [9,10], while here the peak occurs at only $2/3$ the cylinder height. Castro et al. [9] and Coceal et al. [10] investigated the flow over a roughness array with $H/\delta = 0.14$ and an area density of 25%. Even though the H/δ values are similar to those investigated here, the blockage created by their array of elements (surface area density of 25%) was enough to influence the flowfield significantly. The flow over a dense canopy or roughness array contains a strong shear region at the element height, which resembles a mixing layer; this results in a significantly different flowfield from that observed here.

Figures 7–9, show the development of the flow downstream of a spanwise array of cylinders with $3D$ spacing, using mean and rms velocity profiles and the normalized frequency spectra at $z^+ = 100$, respectively. Measurements both directly downstream of the reference cylinder, $y/D = 0$, and at midspacing, $y/D = 1.5$ (or $1.5D$ offset), are shown in these figures. Also, measurements directly downstream of the neighboring cylinder, $y/D = 3$, are included to document repeatability along the span.

In Fig. 7, at $x/D = 4$, the mean velocity profiles directly downstream of the cylinders, $y/D = 0$ and $y/D = 3$ and at $y = 1.5D$ offset (midspacing) match that seen directly downstream of a single cylinder within uncertainty (see Fig. 2a). At zero offset, the deficit in the mean velocity decreases with downstream distance, in the same manner as for the velocity deficit directly downstream of the single cylinder. At $1.5D$ offset, however, the velocity deficit remains approximately constant from $x/D = 4$ to $x/D = 8$, indicating that this spanwise spacing, $3D$, results in a longer-lasting wake with a maximum velocity deficit located midway between the cylinders. This result agrees with the findings of Tomkins [8] that closely spaced hemispheres ($1.3D$ spacing and $H/\delta = 0.09$) in a turbulent boundary layer also exhibited maximum velocity deficit at the midspacing location up to $5D$ downstream. Tomkins [8] suggested that the velocity deficit is generated by hairpin vortices that are either shed from the elements or modified by them. On the other hand, Park and Lee [26], who investigated the effect of spanwise spacing on the flow downstream of two side-by-side cylinders with $H/D = 6$ embedded in a turbulent boundary layer with $H/\delta \sim 0.85$, found that for the largest spacing investigated,$2D$, there was no interaction between the individual wakes at the half cylinder height. It is possible that large H/δ decreases the potential for the spanwise interactions observed in the present data, and perhaps Tomkins [8] could have observed wake interaction at a much larger spacing than $1.3D$ because of their low H/δ.

The results presented in Fig. 7, can also be contrasted with the results of Zhou et al. [6], who examined cylinders with $3D$ spanwise spacing in a uniform, nonturbulent, flow. Zhou et al. [6] found that the individual cylinder wakes remained distinct (with local velocity maximized at midspacing position) until $x = 40D$ downstream.

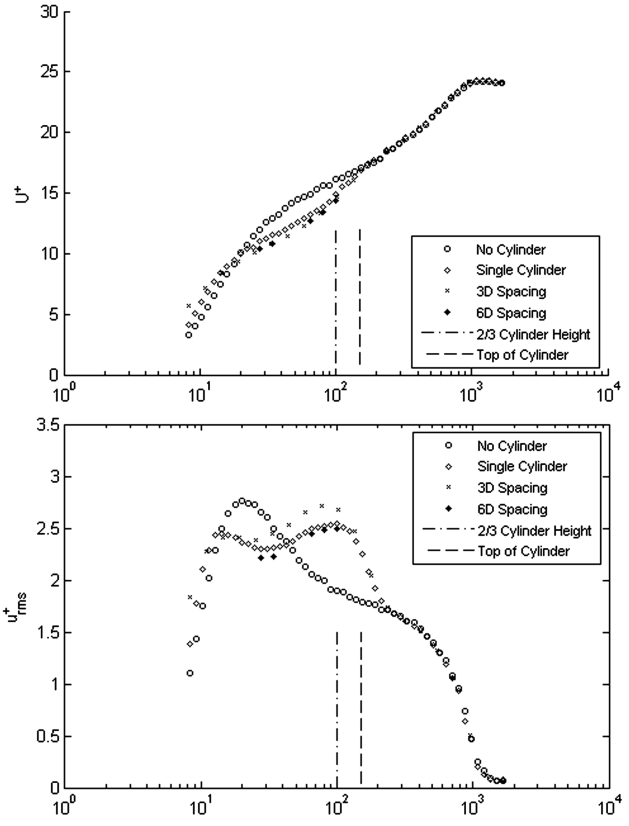

a) No offset, $y/D = 0$

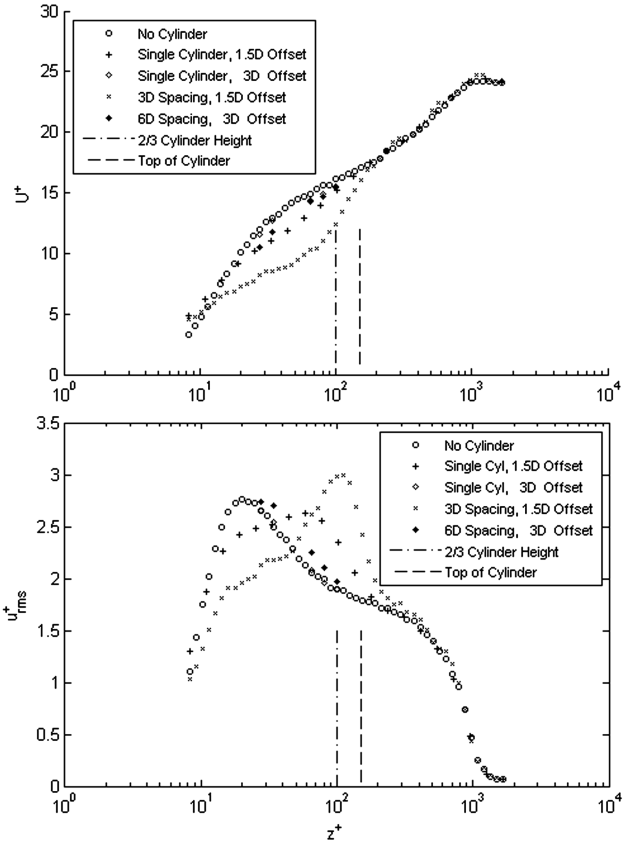

b) With spanwise offset

Fig. 6 Mean and rms velocity profiles behind cylinder arrays at $x/D = 6$. Single-cylinder data are included for comparison.

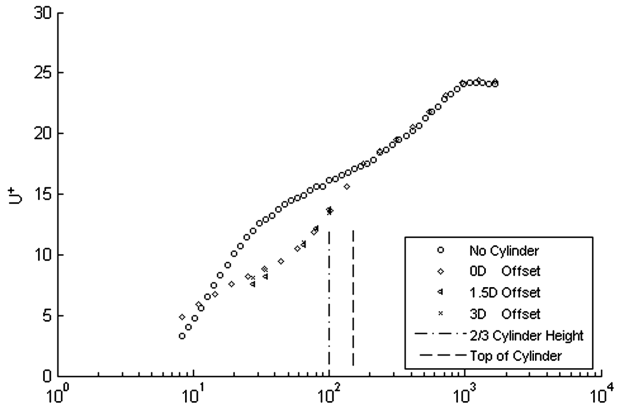

a) $x/D = 4$

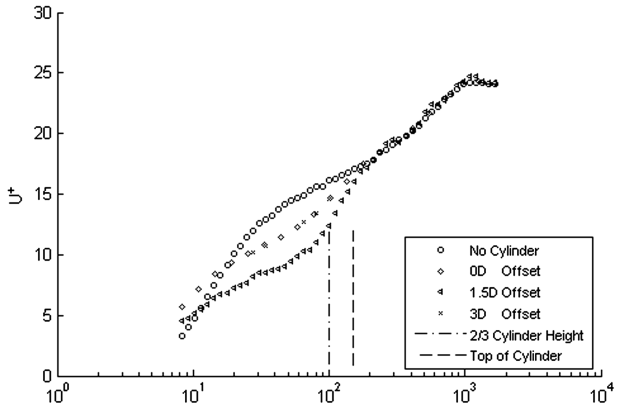

b) $x/D = 6$

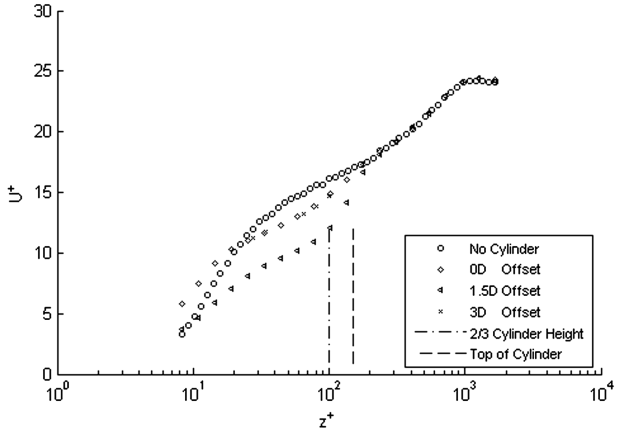

c) $x/D = 8$

Fig. 7 Mean velocity profiles behind a cylinder array with 3*D* spanwise spacing at various downstream locations and spanwise offsets.

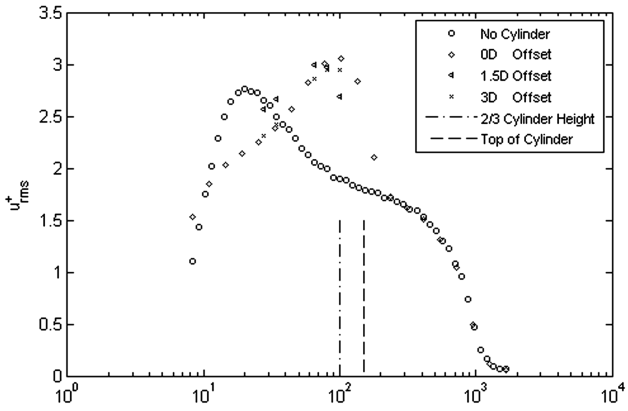

a) $x/D = 4$

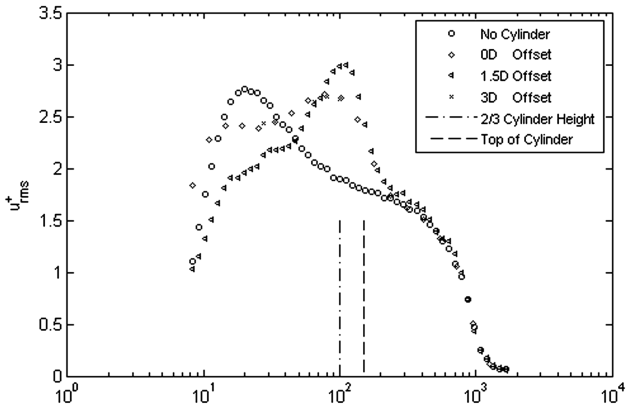

b) $x/D = 6$

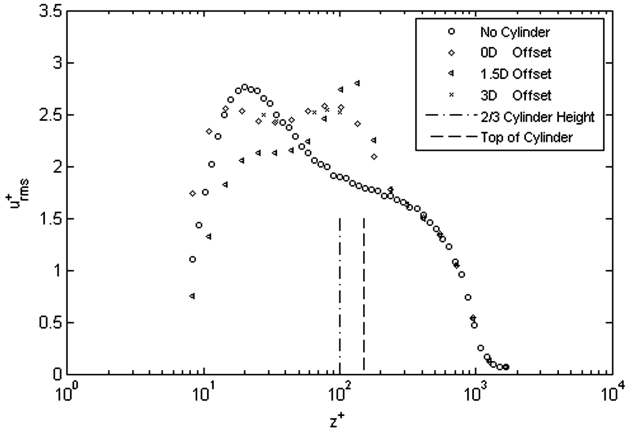

c) $x/D = 8$

Fig. 8 RMS velocity profiles behind a cylinder array with 3*D* spanwise spacing at various downstream locations and spanwise offsets.

Furthermore, those authors showed that reducing the spacing to $1.5D$ induced a wake with a single peak sooner than $10D$ downstream, which agrees better with the current results for $3D$ spacing. In the current results, it is clear then that the turbulent boundary layer extends the spanwise distance over which wake interaction may occur. Assuming that a horseshoe vortex is initiated upstream of each cylinder due to the cylinder/wall interaction there, the legs of the horseshoe would be induced to move outward in the spanwise direction due to the presence of image vortices beneath the wall. This induced motion would extend the range of spanwise interaction compared with any case lacking the wall boundary. In addition, the range of eddy scales present in the turbulent boundary layer as opposed to a relatively quiescent freestream may promote mixing and eddy interactions and thus cause larger regions of the flow to be affected.

In Fig. 8, directly downstream of the cylinders in the $3D$ array, the rms velocity profiles generally agree with those of their single-cylinder counterparts (Fig. 2b) at $y/D = 0$: the rms velocity profile exhibits a peak of larger magnitude near $z^+ = 100$ and a reduction in rms velocity near $z^+ = 20$ relative to the undisturbed case. As downstream distance increases, i.e., at $x/D = 6$ and 8, the rms peak at $z^+ = 100$ decreases and the peak at $z^+ = 20$ begins to return toward the undisturbed condition. However, at midspacing ($y/D = 1.5$), the rms velocity develops differently. At $x/D = 4$ (Fig. 8a), the rms profile at $y/D = 1.5$ appears to peak closer to the wall, around $z^+ = 65$, compared with the profiles directly downstream of the cylinders ($y/D = 0$). At $x/D = 6$ (Fig. 8b), the rms velocity profile at $y/D = 1.5$ has a peak near $z^+ = 100$, with significantly higher magnitude compared with the maximum value observed at $y/D = 0$. At $x/D = 8$ (Fig. 8c), the peak at $y/D = 1.5$ appears to remain very

similar in shape to that observed at $x/D = 6$ with slightly lower value near the 2/3 cylinder height ($z^+ = 100$) and similar magnitudes near $z^+ = 20$. For all streamwise and spanwise locations, the increase in rms velocity extends only to the top of the log region.

Figure 9 shows the normalized frequency spectra at $z^+ = 100$ at $x/D = 6$ directly downstream of the cylinders ($y/D = 0$) and at $y/D = 1.5$. The higher normalized power spectral density at lower frequencies for the $1.5D$ offset compared with zero offset agrees with the significantly higher peak in the rms profile at midspacing. Unlike the single-cylinder case, no dominant frequency was observed for the cylinder array at any of the measured spanwise locations. The integral length scales at $z^+ = 100$ for the zero offset and the $1.5D$ offset are approximately $L^+ = 250$–300, or 2.5 to 3 cylinder diameters, similar to those observed with the single cylinder whenever there was a clear alteration of the mean or rms velocity from the undisturbed value (where L^+ was 400). It should be noted that the data recording time for these spectra was insufficient to accurately resolve content at lower frequencies such as potential low-frequency meandering of low-speed wakes that may eventually evolve into or be associated with vortex packets [30].

To investigate the effects of spanwise spacing further, additional measurements were taken for the array with $6D$ spanwise spacing farther downstream. Figure 10 shows mean and rms velocity profiles behind cylinder arrays with $6D$ spanwise spacing at $x/D = 12$ and at various spanwise offsets. In discussing Fig. 6, it was concluded that at $x/D = 6$ the $6D$ array behaved like independent single cylinders. However, Fig. 10a shows a clear mean velocity deficit at the midspacing location ($y/D = 3$) for $x/D = 12$ that is larger than any observed at $x/D = 8$ behind a single cylinder (Fig. 3c), while the profile at $y/D = 0$ largely resembles the undisturbed condition except in the near-wall region, which will be discussed in the next paragraph. The profiles shown in Fig. 10a suggest that neighboring wakes have at this point interacted to produce a stronger deficit than would be possible with a single cylinder. In Fig. 10b, the rms velocity profile at $y/D = 0$ is similar in shape to that seen at $x/D = 8$ directly behind a single cylinder (Fig. 4c) but with less deviation from the undisturbed case. At the midspacing ($y/D = 3$), the rms values in the log region are slightly higher than those at $y/D = 0$. Thus, the interaction observed for the $6D$ array, which occurs farther downstream than that observed for the $3D$ array, yields weaker effects on the mean and rms velocity profiles compared with the $3D$ array.

In most of the perturbed mean velocity profiles, most noticeably in Fig. 10a, there is an observable rise in velocity in the near-wall region. Directly downstream of the cylinders, this surplus could be caused by a downwash that carries faster-moving fluid from the log region into the near-wall region. However, the effect is seen not only directly downstream of cylinders, but also at spanwise offsets from both the single cylinder and the cylinder arrays. In this case, the rise is limited to the near-wall region resulting in a shallower profile near the wall. A possible explanation is that the previously mentioned downwash should cause a local outflow in the spanwise direction

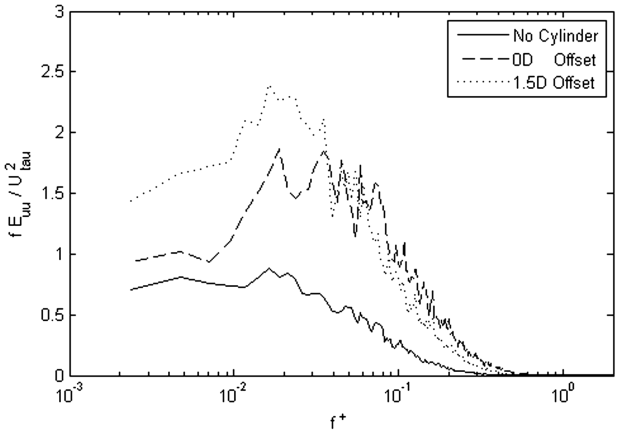

Fig. 9 Normalized frequency spectra behind a cylinder array with $3D$ spanwise spacing at $z^+ = 100$, $x/D = 6$ and various spanwise offsets.

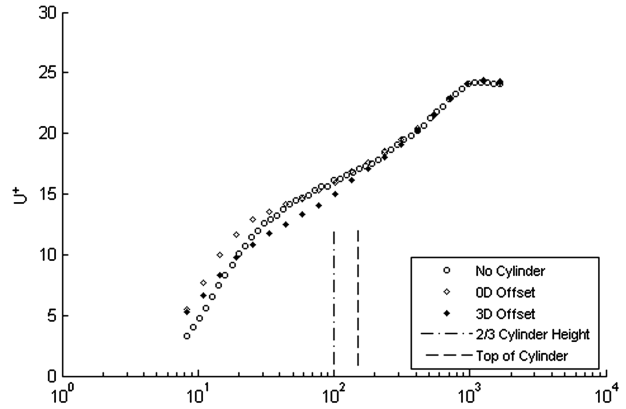

a) Mean velocity

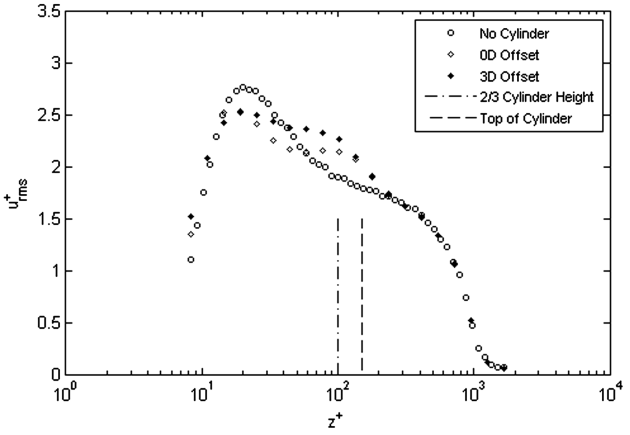

b) RMS velocity

Fig. 10 Mean and rms velocity profiles behind cylinder arrays with $6D$ spanwise spacing at $x/D = 12$ and various spanwise offsets.

away from the cylinder axis and possibly an upwash at midspacing in the case of the arrays. Therefore, faster-moving fluid from the log region would be carried down toward the wall behind the cylinder, and then out along it in the spanwise direction. In the case of the arrays, an upwash at the midspacing would bring slower-moving fluid up from the wall yielding a shallower profile near the wall.

It is interesting to note that in this study ($Re_\tau = 1200$), the perturbations to the velocity field extended to the top of the log region or 4/3 the cylinder height H. In Tomkins's study [8] ($Re_\tau = 2200$), the perturbations to the velocity field at similar streamwise locations extended to $2H$, which also corresponded to approximately the top of the log region. This raises the question of whether the element height, the spacing between elements, and the downstream distance over which wake and eddy interactions and thus turbulent boundary manipulation might occur are a function of outer scales, such as the boundary-layer thickness δ or a function of inner scales u_τ/ν.

The effects of cylinder diameter and height were investigated by examining flow downstream of cylinders with reduced diameter and height. Figure 11 shows mean and rms velocity profiles behind cylinder arrays with $6D$ and $6D_2$ spanwise spacing at $x/D = 12$, $y/D = 3$ and $x/D_2 = 12$, $y/D_2 = 3$, respectively, such that relative to the cylinder diameter used in each test, the array spacings and measurement positions are the same. Profiles were taken with cylinders of $D_2^+ = 50$ (half the original diameter) and heights of both $H^+ = 150$ (AR = 3.0) and $H_2^+ = 100$ (AR = 2.0). A profile for the original $6D$ spaced array, with $D^+ = 100$, measured at the midspacing ($y/D = 3$) was replotted from Fig. 10. Figure 11a shows that despite these changes to the physical dimensions of the cylinders, the resultant streamwise mean velocity profiles are very similar. This suggests, at least for this one case, that the cylinder diameter is an important scaling parameter. Figure 11a also suggests that similar perturbations to mean velocity profiles can be obtained

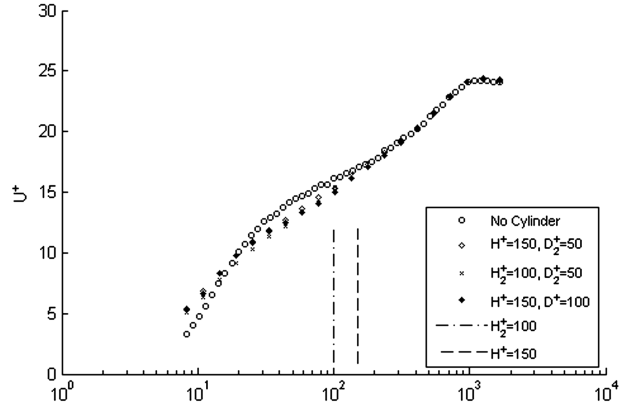

a) Mean velocity

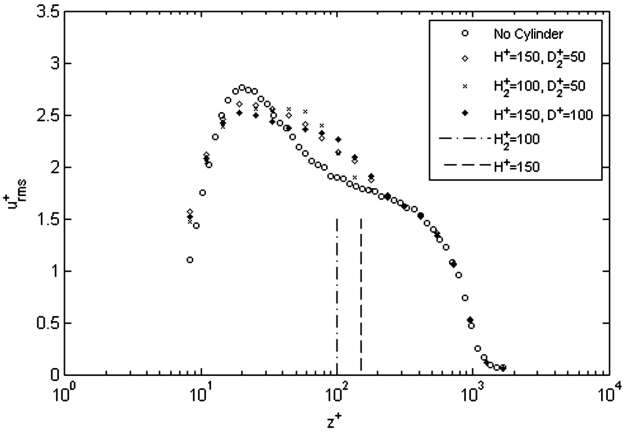

b) RMS velocity

Fig. 11 Mean and rms velocity profiles behind cylinder arrays with $6D$ and $6D_2$ spanwise spacing at $x/D = 12$, $y/D = 3$ and $x/D_2 = 12$, $y/D_2 = 3$, respectively, for multiple cylinder heights. The data labeled "$H^+ = 150$, $D^+ = 100$" are the same as those labeled "$3D$ Offset" in Fig. 10. The other data are based on cylinders with half the diameter, $D_2^+ = 50$; therefore, the physical spacing of the cylinders ($6D_2$) and the downstream measurement location ($x/D_2 = 12$) are half of those in the usual $6D$ spacing arrangement. This difference is shown in Fig. 1c, where all dimensions are given in terms of D, rather than D_2.

with cylinders of smaller height and that those perturbations again extend nearly to the top of the log region. Figure 11b shows that the rms velocity profiles are also very similar, with the shorter cylinders displaying smaller rms values near the top of the log region and higher values around $z^+ = 50$ than for the other two cases.

Conclusions

Mean and rms velocity profiles, as well as normalized frequency spectra and integral length scales were measured downstream ($4 \leq x/D \leq 12$) of a single cylinder and spanwise arrays of cylinders with $3D$ and $6D$ spacing that were fully immersed in a turbulent boundary layer with $Re_\theta = 2800$ ($Re_\tau = 1150$). The cylinders, which had AR $= 1.5$ ($D^+ = 100$), extended well into the log region, $H/\delta = 0.13$ ($H^+ = 150$) of the turbulent boundary layer. Two additional tests used cylinders of $D_2^+ = 50$, $H^+ = 150$ (AR $= 3.0$) and $D_2^+ = 50$, $H_2^+ = 100$ (AR $= 2.0$). For both the single cylinder and the cylinder arrays, the effects on the mean and rms velocities are limited mainly to the log region: $20 < z^+ < 200$ ($z/H < 4/3$).

1) For the single cylinder, aside from the mean velocity deficit in the wake, the main effect is a shift in distribution of the local rms values yielding a peak at $z^+ = 100$ (the $2/3$ cylinder height) and a decrease at $z^+ = 20$. This redistribution of rms velocity away from the wall toward the top of the cylinder but not beyond the top of the log region, with a corresponding increase in the normalized power spectral density over a broad frequency range, was observed up to $8D$ downstream and $4D$ in the spanwise direction.

2) For the cylinder arrays, cylinders with $6D$ spanwise spacing behave like independent elements and the velocity profiles resemble those behind a single cylinder up to $x/D = 6$. Farther downstream, at $x/D = 12$, a weak but definite wake interaction was observed at the midspacing location. However, for the array with a $3D$ spanwise spacing, a large mean velocity deficit at the midspacing location occurs already at $x/D = 4$. The velocity deficit at midspacing for the $3D$ array is much larger than the deficit found downstream of a single cylinder, and it is maintained for at least $8D$ downstream of the cylinders. These results suggest that eddy interactions within the boundary layer lead to broader spanwise interactions than those occurring in wakes of cylinder arrays in a uniform cross flow.

3) A significant peak was observed in the normalized frequency spectrum near the spanwise edge of a single-cylinder wake but no related peak was observed directly downstream of or at any of the measured locations behind the cylinder arrays. Also, perturbations to the velocity profiles do not extend above the log region or $4/3$ the cylinder height. This result suggests that neither tip vortex shedding nor Kármán vortex shedding play strong roles in the downstream flow evolution. On the other hand, it is possible that the horseshoe vortex system at the base of the cylinders does affect the wake interaction and the streamwise distance at which it first occurs. More detailed measurements are needed to explore this possibility.

4) Decreasing the cylinder diameter from $D^+ = 100$ to $D_2^+ = 50$ while maintaining a similar spacing-to-diameter ratio and diameter-referenced measurement position produces a similar perturbation to the mean and rms velocity profiles. That is, in at least one case, the cylinder diameter is the most relevant scaling parameter. Additionally, decreasing the cylinder height by from $H^+ = 150$ to $H_2^+ = 100$ results in smaller rms values near the top of the log region although the perturbations still extend nearly to the top of the log region.

The results presented here suggest that for low values of H/δ, but also H/δ values within the log region, wake interaction can occur for relatively large spanwise spacing (by $x/D = 4$ for $3D$ spanwise spacing and by $x/D = 12$ for $6D$ spacing as shown in the current study). By contrast, if the measurement locations are scaled with the boundary-layer thickness, the current measurements were carried out over a downstream distance of only $0.35 < x/\delta < 1.06$, and thus it is clear that measurements further downstream are needed to investigate longer-term interactions or effects, similar to those observed in [15–19]. Additional questions that arise from the results presented here are as follows: What is the nature of the coherent structures that might be generated by the cylinders and how do they act to alter the eddy organization in a smooth-wall turbulent boundary layer? That is, what causes the peak in rms velocity at midspacing and why do the effects not exceed the top of the log region? More detailed investigations are needed to answer these questions. A possible approach is to use PIV techniques to obtain two- or three-dimensional instantaneous velocity fields and to investigate how coherent vortical structures are modified by cylinder arrangements with characteristics similar to those investigated here.

Acknowledgments

The authors gratefully acknowledge support from the National Science Foundation through grant CBET-0933341 and from the Institute for Mathematics and its Applications at the University of Minnesota.

References

[1] Panton, R. L., "Overview of the Self-Sustaining Mechanisms of Wall Turbulence," *Progress in Aerospace Sciences*, Vol. 37, No. 4, 2001, pp. 341–383. doi:10.1016/S0376-0421(01)00009-4

[2] Adrian, R. J., Meinhart, C. D., and Tomkins, C. D., "Vortex Organization in the Outer Region of the Turbulent Boundary Layer," *Journal of Fluid Mechanics*, Vol. 422, Nov. 2000, pp. 1–54. doi:10.1017/S0022112000001580

[3] Tomkins, C. D., and Adrian, R. J., "Spanwise Structure and Scale Growth in Turbulent Boundary Layers," *Journal of Fluid Mechanics*, Vol. 490, Sept. 2003, pp. 37–74. doi:10.1017/S0022112003005251
[4] Ganapathisubramani, B., Longmire, E. K., and Marusic, I., "Characteristics of Vortex Packets in Turbulent Boundary Layers," *Journal of Fluid Mechanics*, Vol. 478, March 2003, pp. 35–46. doi:10.1017/S0022112002003270
[5] Williamson, C. H. K., "Vortex Dynamics in the Cylinder Wake," *Annual Review of Fluid Mechanics*, Vol. 28, Jan. 1996, pp. 477–539. doi:10.1146/annurev.fl.28.010196.002401
[6] Zhou, Y., Zhang, H. J., and Yiu, M. W., "The Turbulent Wake of Two Side-by-Side Circular Cylinders," *Journal of Fluid Mechanics*, Vol. 458, May 2002, pp. 303–332. doi:10.1017/S0022112002007887
[7] Simpson, R. L., "Junction Flows," *Annual Review of Fluid Mechanics*, Vol. 33, Jan. 2001, pp. 415–443. doi:10.1146/annurev.fluid.33.1.415
[8] Tomkins, C. D., "The Structure of Turbulence over Smooth and Rough Walls," Ph.D. Thesis, University of Illinois at Urbana–Champaign, Urbana, IL, June 2001, pp. 375, 6552.
[9] Castro, I. P., Cheng, H., and Reynolds, R., "Turbulence over Urban-Type Roughness: Deductions from Wind-Tunnel Measurements," *Boundary-Layer Meteorology*, Vol. 118, No. 1, 2006, pp. 109–131. doi:10.1007/s10546-005-5747-7
[10] Coceal, O., Dobre, A., Thomas, T. G., and Belcher, S. E., "Structure of Turbulent Flow over Regular Arrays of Cubical Roughness," *Journal of Fluid Mechanics*, Vol. 589, October 2007, pp. 375–409. doi:10.1017/S002211200700794X
[11] Jiménez, J., "Turbulent Flows over Rough Walls," *Annual Review of Fluid Mechanics*, Vol. 36, Jan. 2004, pp. 173–196. doi:10.1146/annurev.fluid.36.050802.122103
[12] Duriez, T., Aider, J. L., and Wesfreid, J. E., "Self-Sustaining Process through Streak Generation in a Flat-Plate Boundary Layer," *Physical Review Letters*, Vol. 103, No. 14, 2009, p. 144502. doi:10.1103/PhysRevLett.103.144502
[13] Wilkinson, S. P., Anders, J. B., Lazos, B. S., and Bushnell, D. M., "Turbulent Drag Reduction Research at NASA Langley-Progress and Plans," *International Journal of Heat and Fluid Flow*, Vol. 9, No. 3, Sept. 1988, pp. 266–277. doi:10.1016/0142-727X(88)90037-9
[14] Anders, J. B., Jr., "Outer Layer manipulators for Turbulent Drag Reduction," *Progress in Astronautics and Aeronautics: Viscous Drag Reduction in Boundary Layers*, edited by D. M. Bushnell and, J. N. Hefner, Vol. 123, AIAA, Washington, D.C., 1990, pp. 128–143.
[15] Corke T. C., Guezennec Y., and Nagib, H. M., "Manipulation in Drag of Turbulent Boundary Layers Resulting from Manipulation of Large-Scale Structures," *Progress in Astronautics and Aeronautics: Viscous Flow Drag Reduction*, edited by G. R. Hough, Vol. 72, AIAA, New York, 1980, pp. 128–143.
[16] Corke T. C., Guezennec Y., and Nagib H. M., "Modification in Drag of Turbulent Boundary Layers Resulting from Manipulation of Large-Scale Structures," NASA CR-3444, July 1981.
[17] Wark, C. E., Naguib, A. M., and Nagib, H. M., "Effect of Plate Manipulators on Coherent Structures in a Turbulent Boundary Layer," *AIAA Journal*, Vol. 28, No. 11, 1990, pp. 1877–1884. doi:10.2514/3.10494
[18] Guezennec, Y. G., and Nagib, H. M., "Mechanisms Leading to Net Drag Reduction in Manipulated Turbulent Boundary Layers," *AIAA Journal*, Vol. 28, No. 2, 1990, pp. 245–252. doi:10.2514/3.10381
[19] Schofield, W. H., and Logan, E., "Viscous Flow Around Two and Three Dimensional Wall Mounted Obstacles," *1st ASME, SIAM, and APS, National Fluid Dynamics Congress*, AIAA, Washington, D.C., 1988, pp. 1742–1748; also AIAA Paper 1988-3719, 1988.
[20] Sumner, D., Heseltine, J. L., and Dansereau, O. J. P., "Wake Structure of a Finite Circular Cylinder of Small Aspect Ratio," *Experiments in Fluids*, Vol. 37, No. 5, 2004, pp. 720–730. doi:10.1007/s00348-004-0862-7
[21] Wang, H. F., Zhou, Y., Chan, C. K., and Lam, K. S., "Effect of Initial Conditions on Interaction Between a Boundary Layer and a Wall-Mounted Finite-Length Cylinder Wake," *Physics of Fluids*, Vol. 18, No. 6, June 2006, Paper 065106. doi:10.1063/1.2212329
[22] Sakamoto, H., and Arie, M., "Vortex Shedding from a Rectangular Prism and a Circular Cylinder Placed Vertically in a Turbulent Boundary Layer," *Journal of Fluid Mechanics*, Vol. 126, Jan. 1983, pp. 147–165. doi:10.1017/S0022112083000087
[23] Park, C. W., and Lee, S. J., "Flow Structure Around a Finite Circular Cylinder Embedded in Various Atmospheric Boundary Layers," *Fluid Dynamics Research*, Vol. 30, No. 4, 2002, pp. 197–215. doi:10.1016/S0169-5983(02)00037-0
[24] Hain, R., Kähler, C. J., and Michaelis, D., "Tomographic and Time Resolved PIV Measurements on a Finite Cylinder Mounted on a Flat Plate," *Experiments in Fluids*, Vol. 45, No. 4, 2008, pp. 715–724. doi:10.1007/s00348-008-0553-x
[25] Castro, I. P., and Robins, A. G., "The Flow Around a Surface-Mounted Cube In Uniform and Turbulent Streams," *Journal of Fluid Mechanics*, Vol. 79, Feb. 1977, pp. 307–335. doi:10.1017/S0022112077000172
[26] Park, C. W., and Lee, S. J., "Flow Structure Around Two Finite Circular Cylinders Located in an Atmospheric Boundary Layer: Side-by-Side Arrangement," *Journal of Fluids and Structures*, Vol. 17, No. 8, 2003, pp. 1043–1058. doi:10.1016/S0889-9746(03)00070-7
[27] Kline, S. J., and McClintock, F. A., "Describing Uncertainties in Single-Sample Experiments," *Mechanical Engineering*, Vol. 75, No. 1, 1953, pp. 3–8.
[28] Pope, S. B., *Turbulent Flows*, Cambridge University Press, New York, 2000, p. 286, 306–309.
[29] Wei, T., and Willmarth, W. W., "Reynolds-Number Effects on the Structure of a Turbulent Channel Flow," *Journal of Fluid Mechanics*, Vol. 204, July 1989, pp. 57–95. doi:10.1017/S0022112089001667
[30] Hutchins, N., and Marusic, I., "Evidence of Very Long Meandering Features in the Logarithmic Region of Turbulent Boundary Layers," *Journal of Fluid Mechanics*, Vol. 579, May 2007, pp. 1–28. doi:10.1017/S0022112006003946

A. Naguib
Associate Editor